CRYSTAL GROWTH & DESIGN
2006
VOL. 6, NO. 12
2643−2647

Selective Growth of Crystalline SnO_2 on the Polar Surface of ZnO Nanobelts

Jianwei Zhao,* Changhui Ye, Xiaosheng Fang, Lirong Qin, and Lide Zhang

Key Laboratory of Materials Physics, Institute of Solid State Physics, Chinese Academy of sciences, Hefei 230031, P. R. China

Received July 11, 2006; Revised Manuscript Received September 17, 2006

ABSTRACT: A novel nanostructure of a side-to-side SnO_2/ZnO/SnO_2 triaxial nanobelt has been achieved via a simple oxidation of the separated Zn and Sn powders. Each nanobelt has a broad inner ribbon of ZnO with two symmetric SnO_2 sides, and all of the belts are single crystal. This composite structure demonstrates the possibility of selective growth based on the polar surface and also suggests that heterogeneous growth can proceed on both polar surfaces of ZnO ±(0001). The corresponding room-temperature photoluminescence has also been tailored and been discussed in this paper. Our approach presented here would be helpful in designing and preparing many other heterostructures to meet the growing demands of nanoscale science and technology.

Solid-state heterostructures are an integral part of the modern electronic and electro-optic device landscape because of their important electronic properties. Because of the small size of the nanoscale building blocks, heterostructures with self-assembled growth are highly desirable and provide an attractive alternative method in terms of realizing mesoscopic assembly of nanodevices. They can be prepared directly by growing nanoscale structures with different materials. Recently, novel semiconductor heterostructures in nanoscale have been prepared, such as 3D heterostructure of ZnO/SnO_2,[1] Si/Ge nanowires,[2] ZnO/Zn coaxial nanocables,[3] GaP/GaAsP/GaP nanowires,[4] and Si/ZnS biaxial nanowires,[5] and researchers have demonstrated that they may have many highly promising applications. Nevertheless, most of these products are core−shell structures. Although it is now known that the unique properties of nanomaterials depend sensitively on their shape and size, how to develop a selective growth method for achieving desired heterostructures in nanoscale, especially based on the nanobelts, is still a challenge.

Zinc oxide (ZnO), a semiconductor with a direct wide band gap (3.37 eV at room temperature) and large exciton binding energy (60 meV), is one of the most promising materials for applications in catalysts, sensors, piezoelectric transducers, transparent conductors, and surface acoustic wave devices.[6] The structure of ZnO can be described as a number of alternating planes composed of tetrahedrally coordinated O^{2-} and Zn^{2+} ions, stacked alternately along the *c*-axis. The oppositely charged ions produce positively charged Zn-(0001) and negatively charged O-(000$\bar{1}$) polar surfaces.[6,7] The cation-terminated polar surface is chemically active and can be the self-catalyst for growing saw-tooth structures.[8,9] Polar surfaces can also induce the formation of helical and ringed structures driven by the electrostatic forces.[7,10]

In this paper, we report a side-to-side SnO_2/ZnO/SnO_2 triaxial nanobelt for the first time and demonstrate the possibility of selective growth based on the polar surface. The double-sided structure suggests that the heterogeneous growth can proceed on both of the polar surfaces of ZnO ±(0001). The present results may inspire great interest in exploring other selective growth systems and their potential applications in building blocks for nanodevices in the future.

Our synthesis technique is based on the chemical vapor deposition method. The experiment was carried out in a conventional horizontal tube furnace with a 2 cm inner-diameter alumina tube mounted inside. The purity Zn powder (99.9%, about 0.4 g) was placed in a ceramic boat that was covered with a quartz plate to maintain a higher vapor pressure and then put into the center of the alumina tube. Sn powder (99.5%, about 0.1 g) was placed in another boat that was covered with a Si substrate to act as the deposition substrate and placed orderly downstream in the alumina tube. The distance between Zn and Sn powders was about 12 cm. Under a constant flow of Ar (40 sccm), the furnace was rapidly heated to 1000 °C in 10 min and kept at this temperature for 80 min. After the system was cooled to room temperature, a white wool-like product was observed on the Si wafer.

It should be emphasized that the key step of heterogeneous growth is that the two powders should be placed separately, not mixed. In fact, the configuration used in our experiment requires a certain temperature gradient and concentration gradient, which both have an important effect on the morphology of the final product.[11] When these factors are taken into account for the Sn powder, the short horizontal distance (about 5 mm) between the Sn powder and deposition region is more propitious to keeping a proper concentration of SnO_2 for its growth. The as-synthesized products were characterized and analyzed by scanning electron microscopy ((SEM) JEOL JSM 6700F), high-resolution transmission electron microscopy ((HRTEM) JEOL 2010, operated at 200 kV), and energy-dispersive X-ray spectroscope ((EDS) attached to the HRTEM). Photoluminescence (PL) spectra were obtained using an Edinburgh FLS 920 fluorescence spectrophotometer (Xe 900 lamp with output power of 450 W) at room temperature.

Scanning electron microscopy (SEM) was employed to characterize the morphology of the as-synthesized products. The SEM image (Figure 1a) shows that the general morphology of our products are large-scale, beltlike structures with lengths of several tens of micrometers. Figure 1b is the high-magnification SEM image of several composite nanobelts. It shows that the nanobelts are uniform and have a width of about 1 μm. Careful examination of many nanobelts reveals that the widths are mostly in a range of 500−1500 nm. The thicknesses of the nanobelts can be deduced from the belt imaged edge-on to be about 40−80 nm. Shown in Figure 1c is a representative image that reveals the nanobelt to have a thickness of ∼70 nm. But different from the former reports of nanobelts, the products here have a smooth top−bottom surface with two rough edges, as shown in the inset of Figure 1b; this suggests that these nanobelts may have unusual structures.

To obtain more details about the structure and composition of the individual nanobelt, we applied TEM and EDS measurements; the results are shown in Figure 2. The typical bright-field TEM images in panels a and b of Figure 2 reveal that the nanobelts are straight and that both of them have an evident contrast between the inner ribbon and the two side layers. An investigation of many nanobelts reveals that the proportion of these special nanobelts in the products is about 60−70%. From the TEM images, many dark lines are also observed on the inner ribbon due to bending contours, indicating the thin crystal structure. The width of one side layer of the belt is essentially equal to the other, and most of these distribute within 30−100 nm. These widths of the outer layers change discontinuously along the entire nanobelt, and as a result, the nanobelts seem to have rough edges, as observed in the SEM

* Corresponding author. E-mail: jwzhao@issp.ac.cn.

10.1021/cg060445k CCC: $33.50
Published on Web 11/07/2006

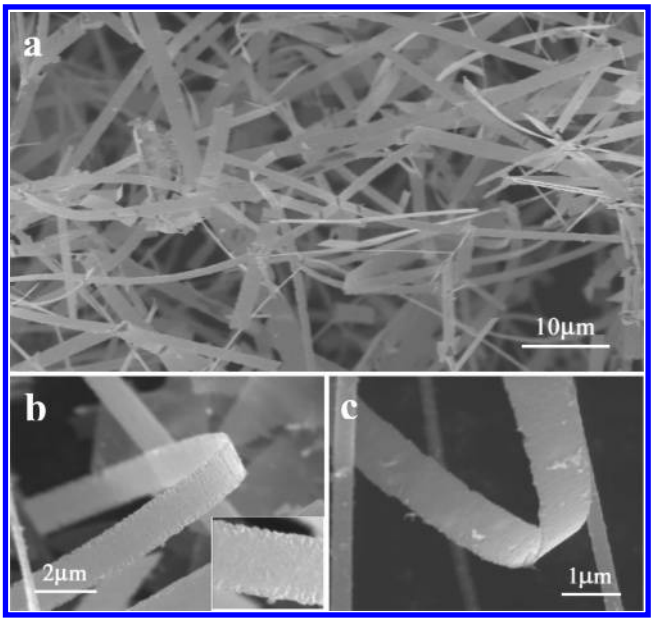

Figure 1. Morphology of the as-synthesized products: (a) low- and (b,c) high-magnification SEM images.

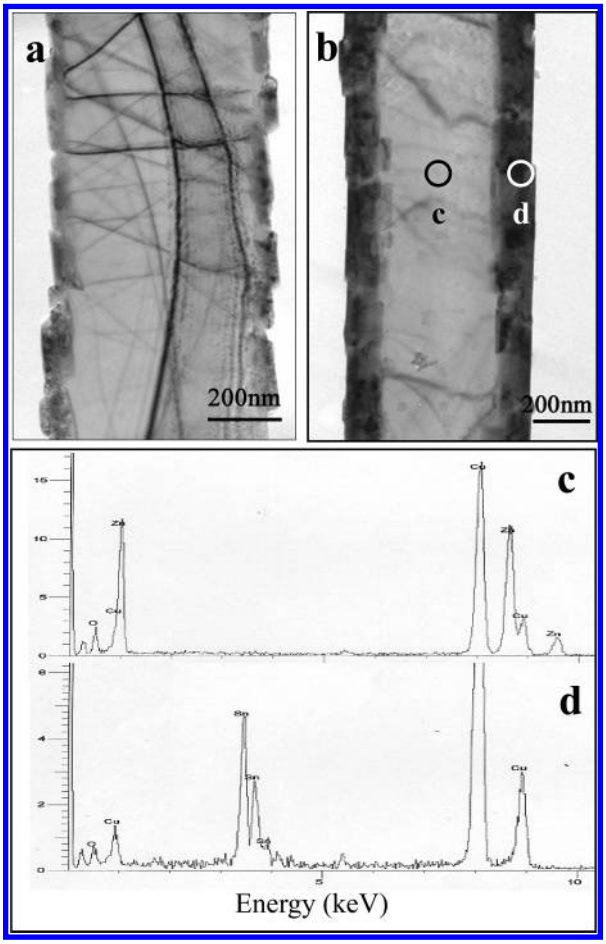

Figure 2. Bright-field TEM images of the single belt with (a) narrow and (b) wide side layers. (c) EDS data of the inner ribbon (indicated by the black ring in Figure 2b) and (d) EDS data of the side layer (indicated by the white ring in Figure 2b), with the Cu peaks coming from the TEM grid.

images. Seen from these two images, the difference in width and roughness of the outer layers should be due to different growth times. Corresponding energy-dispersive X-ray spectroscope (EDS) analysis reveals that the composition of the inner ribbon is Zn and O, whereas the composition of the side area is Sn and O, as shown in panels c and d of Figures 2. The presence of Sn in the two sides but not in the inner ribbon reveals that the nanobelt is not a core−shell structure as usual.

The HRTEM images of the inner ribbon, the interface area, and the side layer are shown in Figure 3a−c, respectively. All of them exhibit clear lattice fringes, which reveal that both the inner ribbon and the side layer are single crystal. The *d*-spacing of the inner ribbon indicated by parallel lines is 0.26 nm, which corresponds to the distance between the (0002) planes of wurtzite ZnO. But the *d*-spacings of the side layers are 0.48 and 0.32 nm, which are close to the distances of the (010) and (001) planes, respectively, of rutile SnO_2. The corresponding SAED patterns of the inner ribbon and the side layer are shown in the panels d and f of Figure 3, which can be indexed for the $[01\bar{1}0]$ zone axis of hexagonal ZnO and the [100] zone axis of tetragonal SnO_2 within experimental error. And both of the above patterns could be observed from the SAED pattern of the interface (Figure 3e). These SAED patterns also reveal that the inner ribbon grows along the $[\bar{2}110]$ direction, with its top−bottom surface $\pm(01\bar{1}0)$ and its side surface $\pm(0002)$, whereas the top−bottom surface and side surfaces of the SnO_2 edges are the $\pm$ (100) and $\pm$ (010) planes, respectively. On the basis of the data presented here, we can determine that the product we synthesized is a structure of side-to-side SnO_2/ZnO/SnO_2 triaxial nanobelts and that it can be described with a model shown in Figure 3h. Because of the nonequilibrium conditions in the process of continuous growth and the lattice mismatches between ZnO and SnO_2, it was possible that the interface between the inner ribbon and outer sides was not a smooth plane. At the interface and its neighborhood, quite a few structural defects (such as misfit dislocations) were observed by HRTEM, similar to Kuang's report.[1] In the present cases, misfit dislocations indicated by arrows in panels b and g of Figure 3 were frequently observed. The formation of such structures is propitious to releasing the increasing stress.

To explore the formation mechanism of these SnO_2/ZnO/SnO_2 nanobelts, we performed another two growth experiments with different heating time durations of 15 and 50 min and with the other parameters essentially the same. In the case of the 15 min duration experiment, the obtained products were the ZnO nanobelts without two SnO_2 sides; a corresponding TEM image is shown in the Figure 4a. When the heating process was extended to 50 min, two thin and discontinuous sides were formed, as seen from Figure 4b. Although some Sn powder was used as the starting material in our experiments, there were no metal particles or other impurities on the tips of the synthesized products, which is the symbol of the VLS model, as analyzed by the SEM and TEM observations. So, the conventional vapor−liquid−solid (VLS) mechanism does not work for the growth of these structures. A possible cause is that the Sn clusters formed in the growth process could be oxidated quickly to SnO_x by the remnant oxygen and lose their catalytic activity.

As we know, there are many reports about preparing ZnO 1D nanostructures by evaporating Zn powder.[12−14] The heating temperature in our experiment reached 1000 °C, which was higher than those of the other reports. This is another important experimental parameter. At this temperature, Zn powder (boiling point: 907 °C) could boil and convert quickly into a mass of Zn vapor. In the mean time, these Zn vapors would be oxidized to ZnO by the remnant oxygen. As a result, there would be a change in supersaturation of ZnO vapor from higher to much lower when the Zn powder was exhausted. Some Sn powder (melting point: 232 °C) was used in our experiment and would be heated to 800 °C, which is higher than the melting point of metal Sn. So in the deposited region, there also would have been quite a few SnO_2 clusters (coming from the oxidation of Sn atoms carried by the Ar). Considering the lower heating temperature and higher boiling point (about 2623 °C), the Sn powder would continue evaporating throughout the experiment to supply the source of SnO_2. On the basis of these analyses and those of two supplementary experiments,

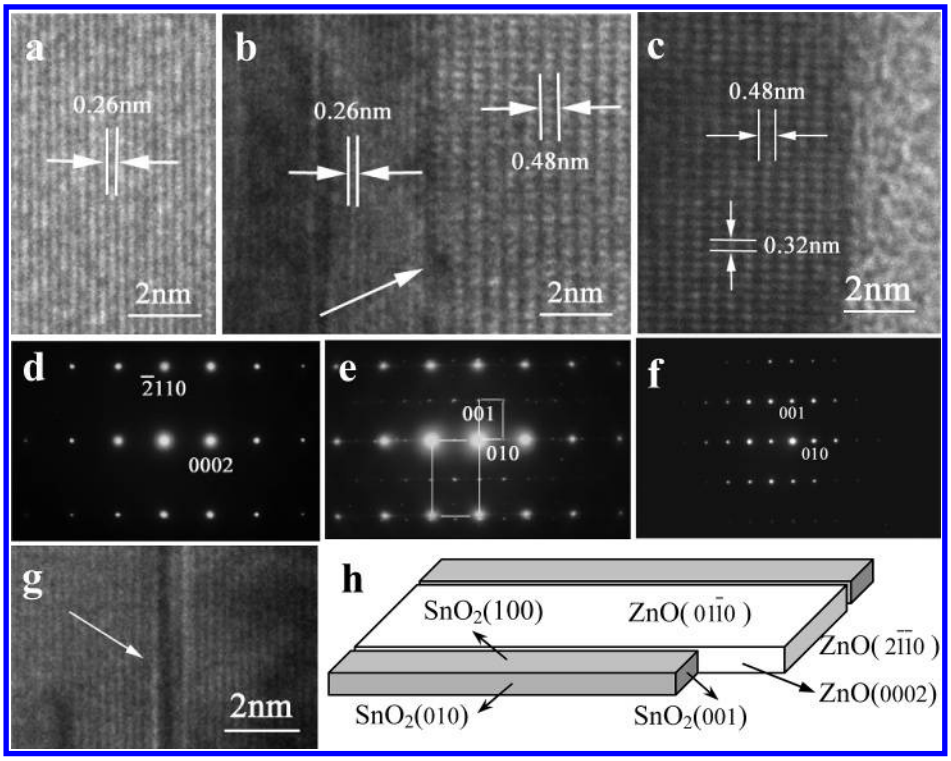

Figure 3. HRTEM image of (a) the inner ribbon, (b) the interface area, and (c) the side layer; corresponding SAED pattern of (d) the inner ribbon, (e) the interface area (e), and (f) the side layer; (g) HRTEM image of the neighborhood of the interface; (h) structure model of the product.

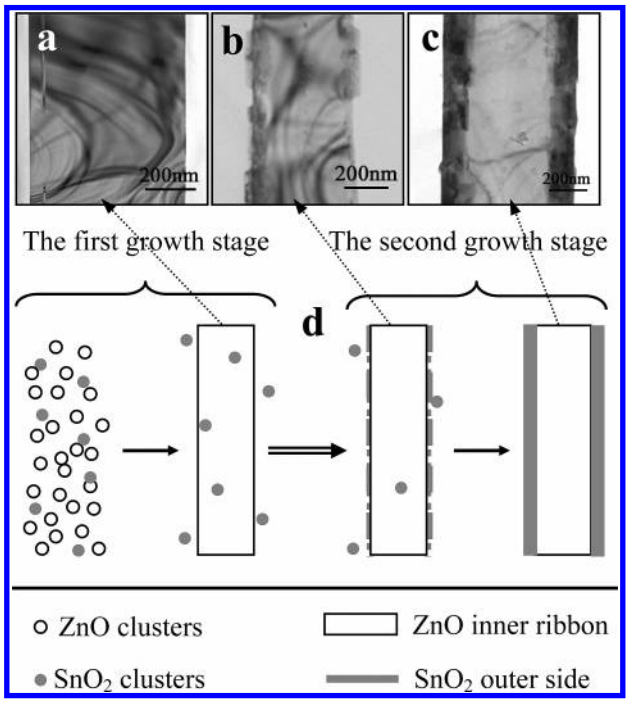

Figure 4. TEM images of the products with heating times of (a) 15, (b) 50, and (c) 80 min; (d) schematic illustration of the growth process of the SnO_2/ZnO/SnO_2 nanobelts.

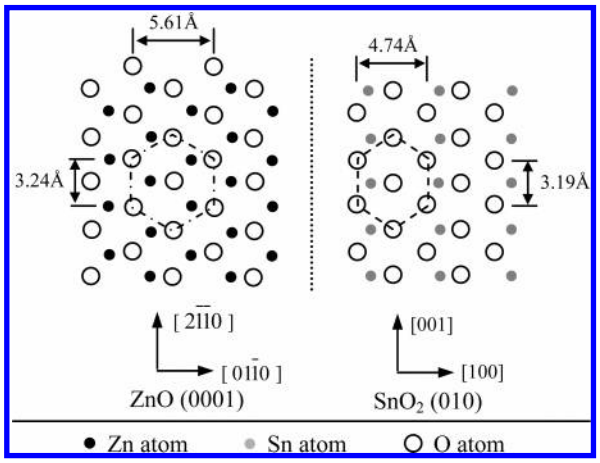

Figure 5. Schematic model of the atomic arrangements on the $(0001)_{ZnO}$ and $(010)_{SnO2}$ planes.

we can separate the formation process of the novel structure presented here into two stages. The schematic diagram for the growth process is illustrated in Figure 4d. The first stage is a fast growth along the $[\bar{2}110]$ direction, forming the inner ribbon of ZnO. This growth behavior was the result of controlling the growth kinetics parameters.[6,15] The high growth rate comes from the high supersaturation of ZnO vapor. And the presence of a few SnO_2 molecules in the first stage probably has little influence on the growth of ZnO.[16] The second stage is a subsequent slower heterogeneous growth along the polar surface of ZnO $\pm(0001)$, creating two SnO_2 sides.

It is reported that, from the point of view of epitaxial relations in their strict meaning, the atomic arrangements of the $(010)_{SnO2}$ plane have very good structural compatibility with that of the $(01\bar{1}0)_{ZnO}$ plane.[1] Here, we demonstrate another feasibility of heterogeneous growth of crystalline SnO_2 on ZnO, as shown in the schematic model of Figure 5. It can be seen that the O atoms in the $(0001)_{ZnO}$ plane take a hexagonal closest-packed arrangement, with a 6-fold symmetry. As for the $(010)_{SnO2}$ plane, O atoms take a pseudo-hexagonal closest-packed arrangement, having a quasi-6-fold symmetry. The lattice (O−O distance) mismatches in the $[2\bar{1}\bar{1}0]_{ZnO}\|[001]_{SnO2}$ and $[01\bar{1}0]_{ZnO}\|[100]_{SnO2}$ directions are 1.8 and 15.5%, respectively. Considering the relation of O atoms, the growth of SnO_2 on the (0001) plane of ZnO is possible. So, it can be concluded that crystalline SnO_2 has the ability to grow on both the $(01\bar{1}0)_{ZnO}$ and $(0001)_{ZnO}$ plane. However, investigation results show that the heterogeneous growth of the $(010)_{SnO2}$ plane in our

experiments was only on the $\pm(0002)_{ZnO}$ plane. The question remaining is what induced the selective nucleation and growth?

Structurally, the $\pm(0002)$ plane belonged to the polar surfaces of the wurtzite structure and always played particular roles in crystal growth. In recent years, a series of unique and novel nanostructures based on the polar surface have been synthesized and investigated, e.g., CdSe nanosaws,[17] ZnS nanosaws,[18] ZnO nanocombs,[9] and ZnO nanosprings.[19] Here, our product is just a structure of SnO_2 outer sides grown on the polar surfaces of the ZnO inner ribbon. So it is thought that the formation of the side-to-side SnO_2/ZnO/SnO_2 triaxial nanobelt is also induced by the polar surfaces. Studies have found that the (0001) face in ZnO crystal was unstable; it tends to grow ledges or steps, which would act as nucleation sites to enhance the growth behavior on the Zn-(0001) surface.[20] Although the (0001)-O surface is chemically inactive and typically does not initiate any growth, controlling experimental conditions could lead to growth from the edges between the $(000\bar{1})$ surface and the $(\bar{2}110)$ planes.[15] Applying these models to our case, the initial nucleation of SnO_2 may be related to the presence of nucleation sites on the two polar surfaces of the ZnO inner ribbon. In addition, the ZnO inner ribbon has polar charges on its two side surfaces. Wang and co-workers have reported a distinct nanoring structure and demonstrated that electrostatic forces coming from the polar charges can drive self-assembly, especially in gas-phase environments.[7] Huang et al. and Zhou et al. further proved that the polar charges of both the ZnO $\pm(0001)$ planes had strong electrostatic interactions with the H_2O molecule or other ions.[21,22] Accordingly, under the conditions of the second growth stage, some SnO_x clusters would be attracted by the electrostatic forces and adsorbed throughout the side surface of ZnO ribbon. As a result, the growth of SnO_2 after its initial nucleation would change to be continuous on the polar surface to form two outer sides. The subsequent self-growth of SnO_2 for a long time could then result in wide and uniform sides (this can be seen from images a and b of Figure 2). Furthermore, it is known that the (0001)-Zn surface tends to have tiny Zn clusters at the growth front, which could result in a fast growth by the self-catalyzed effect to form an asymmetric structure.[15] Different from the literature, for the two outer sides of our product, TEM observations showed that the sides were close to being symmetric in structure. In addition, the HRTEM and EDS analysis indicated that there were no Zn clusters at the laterals of the triaxial nanobelt. So we concluded that self-catalyzed fast growth did not contribute to the formation of our product. The possible cause may be related to the remnant oxygen and the adsorption of SnO_2. It should be mentioned that ZnO has two polar surfaces: {0001} and $\{01\bar{1}1\}$. The former is frequently observed, but the latter is rare.[6,10,22] The composite structure presented here was a selective growth based on the appeared {0001} surfaces. We believe the $\{01\bar{1}1\}$ surfaces also have the ability to induce selective growth in proper conditions.[6] More work is underway to better understand the growth mechanism and to prepare other heterostructures based on the polar surface.

The room-temperature PL spectra of these composite nanobelts are shown in Figure 6 and the excitation wavelength is 325 nm. Compared with the emission of the pure ZnO nanobelts, the SnO_2/ZnO/SnO_2 triaxial nanobelts showed only a much stronger green emission centered at 500 nm, and no obvious UV emission at 382 nm could be seen. It was traditionally deemed that the UV emission corresponded to the near-band-edge (NBE) peak, the green emission originated from the recombination of the holes with electrons occupying the singly ionized O vacancy, and other structural defects or impurities also have an important effect on the luminescence of ZnO nanostructure.[23,24] In our experiment, the condition of lacking oxygen and the reduction of O atoms consumed by Sn would bring more O vacancies to the inner ZnO ribbon. Moreover, the mismatch at two interfacial regions could result in many defects and stacking faults. Both of the above causes would weaken the UV emission and enhance the green emission greatly, resulting in the large difference in the PL from the pure ZnO nanobelts. In the same way, there were also many O vacancies in the two SnO_2 sides, and the interfacial mismatch should affect the sides, too. As a result, the SnO_2 nanostructure always shows a weak yellow emission band.[25,26] This emission was reflected on the PL spectra of our SnO_2/ZnO/SnO_2 nanobelts as a weak shoulder peak at about 590 nm, shown in Figure 6. Compared with the former ZnO/SnO_2 composite nanostructure,[1] our triaxial nanobelts revealed more distinct tailoring to the optical property. The special composite structure accompanied by its optical properties may endow the products presented here with some potential applications in photoelectricity and photocatalysis.[27]

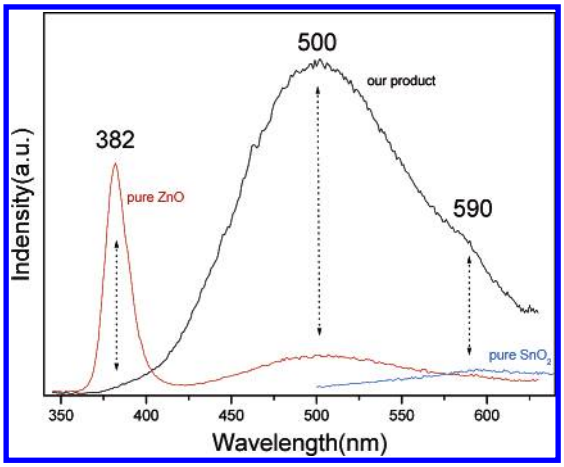

Figure 6. PL spectrum of the composite nanobelts. For comparing, the PL spectra of the pure ZnO and SnO_2 nanobelts are also provided (the excitation wavelength was 325 nm).

In summary, a novel nanostructure of side-to-side SnO_2/ZnO/SnO_2 triaxial nanobelts has been achieved via a simple oxidation of the separated Zn and Sn powders. Each nanobelt has a broad inner ribbon of ZnO with two symmetric SnO_2 sides, and all of the nanobelts are single crystal. The formation of this structure is probably induced by the polar surface of ZnO. The as-synthesized product provides a new candidate for nanodevices. Our approach of selective growth induced by polar surface would be helpful in designing and preparing many other heterostructures to meet the growing demands of nanoscale science and technology.

Acknowledgment. This work was financially supported by the National Major Project of Fundamental Research: Nanomaterials and Nanostructures (Grant 2005CB623603) and the Special Fund for President Scholarship, Chinese Academy of Sciences.

References

(1) Kuang, Q.; Jiang, Z. Y.; Xie, Z. X.; Lin, S. C.; Lin, Z. W.; Xie, S. Y.; Huang, R. B.; Zheng, L. S. *J. Am. Chem. Soc.* **2005**, *127*, 11777.
(2) Lauhon, L. J.; Gudiksen, M. S.; Wang, D.; Lieber, C. M. *Nature* **2002**, *420*, 57.
(3) Wu, J. J.; Liu, S. C.; Wu, C. T.; Chen, K. H.; Chen, L. C. *Appl. Phys. Lett.* **2002**, *81*, 1312.
(4) Svensson, C. P. T.; Seifert, W.; Larsson, M. W.; Wallenberg, L. R.; Stang, J.; Bauer G.; Samuelson, L. *Nanotechnology* **2005**, *16*, 936.
(5) Hu, J.; Bando, Y.; Liu, Z.; Sekiguchi, T.; Golberg, D.; Zhan, J. *J. Am. Chem. Soc.* **2003**, *125*, 11306.
(6) Wang, Z. L. *J. Mater. Chem.* **2005**, *15*, 1021.
(7) Kong, X. Y.; Ding, Y.; Yang, R.; Wang, Z. L. *Science* **2004**, *303*, 1348.
(8) Lao, C .S.; Gao, P. X.; Yang, R. S.; Zhang, Y.; Dai, Y.; Wang, Z. L. *Chem. Phys. Lett.* **2006**, *417* 358.
(9) Fan, H. J.; Scholz, R.; Dadgar, A.; Krost, A.; Zacharias, M. *Appl. Phys. A* **2005**, *80*, 457.
(10) Yang, R. S.; Ding, Y.; Wang, Z. L. *Nano Lett.* **2004**, *4*, 1309.
(11) Ye, C. H.; Fang, X. S.; Hao, Y. F.; Teng, X. M.; Zhang, L. D. *J. Phys. Chem. B* **2005**, *109*, 19758.
(12) Dang, H. Y.; Wang, J.; Fan, S. S. *Nanotechnology* **2003**, *14*, 738.
(13) Umar, A.; Kim, S. H.; Lee, Y. S.; Nahm, K. S.; Hann, Y. B. *J. Cryst. Growth* **2005**, *282*, 131.

(14) Wang, R. C.; Liu, C. P.; Huang, J. L.; Chen, S. J. *Appl. Phys. Lett.* **2005**, *86*, 251104.
(15) Wang, Z. L.; Kong, X. Y.; Zuo, J. M. *Phys. Rev. Lett.* **2003**, *91*, 185502.
(16) Kong, X. Y.; Wang, Z. L. *Appl. Phys. Lett.* **2004**, *84*, 975.
(17) Ma, C.; Ding, Y.; Moore, D.; Wang, X.; Wang, Z. L. *J. Am. Chem. Soc.* **2004**, *126*, 708.
(18) Moore, D.; Ronning, C.; Ma, C.; Wang, Z. L. *Chem. Phys. Lett.* **2004**, *385*, 8.
(19) Gao, P. X.; Wang, Z. L. *Small* **2005**, *1*, 945.
(20) Wang, Y.; Wang, G. Z.; Yau, M. Y.; To, C. Y.; Ng Dickon, H. L. *Chem. Phys. Lett.* **2005**, *407*, 510.
(21) Huang, H.; Yang, S.; Gong, J.; Liu, H.; Duan, J.; Zhao, X.; Zhang, R. *J. Phys. Chem. B* **2005**, *109*, 20746.
(22) Zhou, X.; Xie, Z.; Jiang, Z.; Kuang, Q.; Zhang, S.; Xu, T.; Huang, R.; Zheng, L. *Chem. Commun.* **2005**, 5572.
(23) Vanheusden, K.; Seager, C. H.; Warren, W. L.; Tallent, D. R.; Voigt, J. A. *J. Appl. Phys.* **1996**, *79*, 7983.
(24) Hu, J. Q.; Bando, Y.; Zhan, J. H.; Li, Y. B.; Sekiguchi, T. *Appl. Phys. Lett.* **2003**, *83*, 4414.
(25) Hu, J. Q.; Bando, Y.; Liu, Q. L.; Golberg, D. *Adv. Funct. Mater.* **2003**, *13*, 493.
(26) He, J. H.; Wu, T. H.; Hsin, C. L.; Li, K. M.; Chen, L. J.; Chueh, Y. L.; Chou, L. J.; Wang, Z. L. *Small* **2006**, *2*, 116.
(27) Dodd, A.; McKinley, A.; Saunders, M.; Tsuzuki, T. *Nanotechnology* **2006**, *17*, 692.

CG060445K